

Article

LoRa-Based Wireless Sensors Network for Rockfall and Landslide Monitoring: A Case Study in Pantelleria Island with Portable LoRaWAN Access

Mattia Ragnoli ¹, Alfiero Leoni ¹, Gianluca Barile ^{1,2}, Giuseppe Ferri ¹ and Vincenzo Stornelli ^{1,2,*}

¹ Department of Industrial and Information Engineering, University of L'Aquila, 67100 L'Aquila, Italy
² Design Methodologies of Embedded Controllers, Wireless Interconnect and Systems-on-Chip Center (DEWS), University of L'Aquila, 67100 L'Aquila, Italy
* Correspondence: vincenzo.stornelli@univaq.it

Abstract: Rockfalls and landslides are hazards triggered from geomorphological and climatic factors other than human interaction. The economic and social impacts are not negligible, therefore the topic has become an important field in the application of remote monitoring. Wireless sensor networks (WSNs) are particularly suited for the deployment of such systems, thanks to the different technologies and topologies that are evolving nowadays. Among these, LoRa modulation technique represents a fitting technical solution for nodes communication in a WSN. In this paper, a smart autonomous LoRa-based rockfall and landslide monitoring system is presented. The structure has been operating in Pantelleria Island, Sicily, Italy. The sensing elements are disposed in sensor nodes arranged in a star topology. Network access to the LoRaWAN and the Internet is provided through gateways using a portable, solar powered device assembly. A system overview concerning both hardware and functionality of the nodes and gateways devices, then a power analysis is reported, and a monthly recorded result is presented, with related discussion.

Keywords: wireless sensor network (WSN); monitoring; Internet of Things (IoT); LoRa; rockfall monitoring; energy harvesting; sensors; risk prevention



Citation: Ragnoli, M.; Leoni, A.; Barile, G.; Ferri, G.; Stornelli, V. LoRa-Based Wireless Sensors Network for Rockfall and Landslide Monitoring: A Case Study in Pantelleria Island with Portable LoRaWAN Access. *J. Low Power Electron. Appl.* **2022**, *12*, 47. <https://doi.org/10.3390/jlpea12030047>

Academic Editors: Lan-Da Van, Khanh N. Dang and Kun-Chih Chen

Received: 25 August 2022

Accepted: 6 September 2022

Published: 7 September 2022

Publisher's Note: MDPI stays neutral with regard to jurisdictional claims in published maps and institutional affiliations.



Copyright: © 2022 by the authors. Licensee MDPI, Basel, Switzerland. This article is an open access article distributed under the terms and conditions of the Creative Commons Attribution (CC BY) license (<https://creativecommons.org/licenses/by/4.0/>).

1. Introduction

Landslides and rockfalls are natural hazards linked to the combination of geomorphological and climatic factors in response to triggering mechanisms, such as heavy rainfall or seismic events, vegetation interaction, and human action [1,2]. Due to the rising awareness of economic and social impacts of landslides and rockfalls, the risk control of these events has become a topic of major interest. The effects include economic losses, the threat to human safety, environmental endangerment and impact on the possibility of urbanization [3]. A clear example about the danger of these occurrences is shown by events in combination with transport routes [4], where in addition to damages to infrastructures, there are unfortunately monetary losses due to the service disruption. The interest of the scientific community in the major hazards of these phenomena is well known worldwide, especially in areas where the presence of rock formations or unstable terrains represent a high source of risk [5].

The island of Pantelleria, located between the coasts of southern Sicily (Italy) and Tunisia, represents the emerged part of a volcanic structure. The structure of this island is deforming due to volcanic and tectonic activity [6]. It is necessary to monitor the rockfall and landslide activity along the surfaces of slopes and rock faces for safety purposes and to track the degradation and change of the territory. The morphology of the rocky walls in Pantelleria, especially along coastal areas, makes the development of a wired structural monitoring system difficult. Wireless sensors networks offer an advantageous mechanism for monitoring purposes because it is possible to implement a network of nodes without

wiring, and to use sensing units to gather information. Earlier, engineers have employed wired and single-hop wireless data acquisition systems to acquire useful data for structural monitoring [7,8]. However, power and wiring constraints can combine in increasing the cost and complexity of data acquisition, most importantly by limiting the number and applicable location of sensor nodes. Maintenance and deployment costs can be increased too. Considering these, wireless sensor networks can often help address these issues.

The current trend is to embrace Internet of Things (IoT) paradigms, benefiting from smart nodes to build flexible and powerful infrastructures for data acquisition and analysis. The physical devices equipped with sensing instrumentation are connected to the internet, which allows data exchange between heterogeneous platforms, making the system technology independent from a certain point of the acquisition chain.

In the recent years WSNs have reported a rapid growth thanks to various new technologies for wireless communication, new implementations of ad-hoc hardware devices, and important academic and industrial research effort in this matter [9]. The applications served by wireless networks are various and different [10], including environmental monitoring [11], health related applications, including wearable systems [12], early warning tools [13], and industrial control [14].

Overview on State of the Art Rockfall and Landslide Monitoring Systems

The development of an optimal solution for a monitoring system is an open challenge for different reasons. Determining which of the existing ones is the most appropriate solution is absolutely not trivial. The sensing structures are incredibly heterogeneous in many terms: technology, topology, reliability, cost, and complexity. For the aforementioned reason, it is challenging to find a system that fits them all indiscriminately. Furthermore, due to the multidisciplinary nature of the monitoring topic, taking into account all the variables involved is complicated.

In this section, different solutions for rockfall and landslide monitoring systems, based on wired and wireless networks will be briefly reviewed, so to give a perspective on the state of the art. Employing structural health monitoring (SHM), a connected aspect of the aforementioned phenomena, an overview on WSN-based applications will be reported.

In [15] the authors present a survey of technological developments and research work in the IoT, applied to the prevention of geological hazards. It surveys the applications in the monitoring and early warning of various types of common geohazards: rockfall, surface collapse landslides, and debris flow earthquakes. Some IoT-providing technologies are investigated in geohazards, and the challenges are summarized with an address to future developments in the topic.

Wireless sensor nodes incorporating microelectromechanical system (MEMS) inertial measurement unit (IMU) sensors can be used to detect movements on rock or soil slopes. In [16] the authors present a sensing system able to recognize a rock fall event and to monitor the structural parameters of a protection barrier, which can be a gabion mesh or concrete blocks. The architecture is modular, organized with a control unit and sensing nodes disposed on the installation site. With these devices, information about the vibration and the inclination of the falling rock protection barrier is gathered. The data are collected on a web server which handles recording and automatic messages in case of criticisms. A web application has been developed to create summary reports and to analyze the data collected. The system is currently working on a gabion mesh located in the southern part of Italy.

Despite the ability of the IMU-based WSNs to measure accelerations and rotations, there is a significant research effort to describe and distinguish different types of slope movement. Studies have presented distinct patterns of accelerometer data in physical structures' behavior [17]. The concept of pattern recognition has been utilized in experimental studies that were carried out by the authors using the accelerometer and gyroscope readings to classify movements. This information serves as the fundamental understanding of a landslide in civil engineering, as well as helping in analyzing the stability of the slope

and the implementation of safety and mitigation structures. In [18], the authors present a system based on WSN nodes which communicate with a central station using 802.11 g standard [19]. The station is a trailer equipped with computers for onsite data analysis and cellular uplink. The connection is used for internet communication to a central storage server. Experiments using a rock equipped with a sensor device are carried out and results reported to show the different IMU data for possible movements of the mass. In [20], the authors propose a system based on acoustic emission or microseismic monitoring to provide an insight into stress and strain conditions in the subsurface rock mass. Detecting microseismic events originating from an unstable rock mass is important for locating growing cracks and to analyze the triggering mechanisms of possible future collapses. In [21], a network of sensor nodes based on MEMS analog output accelerometers and MicaZ [22] mote hardware is deployed. Each node is equipped with a microcontroller and a 2.4 GHz transceiver. The devices are mounted in a linear configuration along the Golden Gate Bridge, which makes the multi-hop transmission topology particularly suited for the study. Effort is made to analyze the data transmission reliability in pipeline mode to reduce data loss. The mechanism implemented is as follows: the sender transmits the data when it is requested by the receiver, and the receiver identifies possible missing packets and returns a list back to the sender, which resends those until total reception is achieved. A cycle of data sampling and collection is executed in about 9 h and produces 20 MB of data.

In [23], a disaster prevention system tested in a slope area around Taiwan is shown. Monitoring equipment was installed on the protection structure construction to display quantitative data of rockfall events. The accelerometric nodes prototypes are built on commercially available electronic circuits encapsulated in plastic enclosures and are three different types, each one characterized by a different transmission technology. The first is a long range (LoRa) [24,25]-based node, the second uses narrowband-IoT (NB-IoT) [26] and the third communicates with Long Term Evolution (LTE) M1 [27,28]. The LoRa unit does not use a free access media access control (MAC) layer but communicates data to a Raspberry Pi 3B [29] unit which uses Wi-Fi to later transmit to a MySQL [30] server. There is also a wired vibration gauge, VB-200SC [31], interfaced through RS-485 [32] with an IoT gateway to transmit data over Wi-Fi. In [33], the authors implement a LoRa-based WSN on an uninhabited hillside landslide, studying the feasibility of a LoRa-based network in harsh environments and focusing on the zone coverage of the communication and on received signal strength intensity (RSSI)-based triangulation to localize a particular node in the network. However, we do not find an in-depth description on the hardware implementation of the sensor node, a description of the mounting mechanisms on the slope side, or power-related features of the elements. In [34] the authors propose a landslide-monitoring-method-based LoRa network and intelligent sensing for rainfall and landslide displacement in Shuicheng County, Guizhou Province, China. The general structure, hardware, and software design of the system are described comprehensively. The work reports the possibility, for the nodes, to operate in normal or reduced power mode to obtain a lower current absorption of 1 mA.

An application of a LoRa-based wireless monitoring device for SHM is presented in [35]. In a smart city, Remote Structural Health Monitoring (RSHM) is a perfect solution for tracking critical damage to urban structures. The cited paper proposes TenSense M30, an IoT sensor node to enable wide communication coverage, with a long battery duration, for monitoring the health of bolted joints. TenSense M30 has a footprint that can be used as an add-on to current structures. Hardware and mechanical tests are presented.

In this work a low-cost autonomous LoRa-based rockfall and landslide monitoring system, operating in Pantelleria Island since May 2022, is presented. The sensor nodes are independent elements in a star topology network with the LoRaWAN [36,37] gateway, making the network more robust in case of node malfunction. The access to the internet layer is provided using a compact, portable, solar-powered gateway implementation system. This paper is structured as follows: a system overview is given, with a functionality description. The next section describes the nodes and gateway assembly box with electrical measurements of power performances of the nodes and considerations on its long-term

reliability. A section with a month's recorded data is reported. Finally, conclusions are drawn.

2. System Overview

In IoT-oriented WSNs, it can be beneficial to implement low power wide area network (LPWAN) technologies. This can allow for good energetic performances of the sensor nodes, which is crucial in energy harvesting powered devices [38–40]. Using the emerging LPWAN technologies, an overall inexpensive implementation is achievable [41,42]. In these structures, especially for monitoring purposes, the required data rate is usually lower than high-speed telecommunications applications, such as large file transfers or video streaming. LPWAN are often used in scenarios where a small amount of data is transmitted at intervals of time [43], often leading to less complicated transceiver hardware, hence reduced costs. The MAC layer deployment often comes with the highest costs of the whole system [44], so if a relatively unexpensive solution is provided with respect to the total cost of the system, an optimal point is reached. The LoRaWAN MAC layer, regulated by the LoRa Alliance [45], provides this kind of performance, being a free network protocol accessible by dedicated LoRaWAN gateways. These devices can be found commercially at affordable prices in certificated outdoor models. Such elements can be interfaced with free web services to create a reliable, fully developed, low-cost network, as will be presented later in this paper. The network architecture (see Figure 1), in the aforementioned MAC layer, is organized in a star structure with the gateway acting as the star center. The nodes communicate with a single hop connection using LoRa modulation, which is a chirp spreading spectrum (CSS)-based technique from Semtech, as mentioned in the introduction.

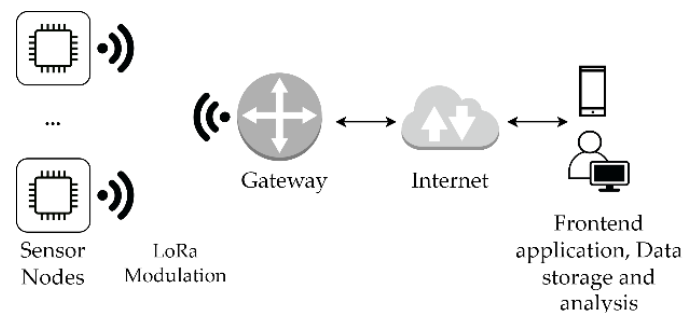


Figure 1. General LoRaWAN network architecture scheme for WSN applications.

In [46] an energetic efficiency comparison between LPWAN IoT devices is available. LoRa has similar power performances to SigFox [47], which does not allow an easier implementation at access layer, as it is LoRaWAN. In [48] we can find how this modulation compares with other IoT-oriented transmission technologies, also reporting good coverage when working in poor link conditions.

The system proposed in this work is as follows: sensor nodes are equipped with MEMS accelerometer, GPS unit for tracking, gas sensor measuring relative humidity, barometric pressure, ambient temperature, and gas resistance which can be used for air quality (AQI) index. The nodes transmit packets of 38 bytes size every 60 min to the gateway through LoRa physical layer. This last element is connected to the internet via IPv4 [49] using LTE by means of a subscriber identity module (SIM), and powered via solar harvesting by means of a solar panel and charge storage battery. A detailed hardware description will be provided in the next section. The packets received at the gateway are managed through The Things Network [50] service, where, using a payload decoding function, the incoming bytes are encapsulated into a JavaScript Object Notation (JSON) object for data exchange between websites. The object has a key-value field and numerical value for each measured quantity. HyperText Transfer Protocol (HTTP) integration is used to send the packets to the Losant IoT [51] website, which acts as a user frontend, database, and alert-triggering service. In this service the obtained data is plotted into a user dashboard and stored into a

database, which is accessible from the monitoring system provider for data analysis. In Figure 2, the application specific block scheme is shown. Each node of the WSN is installed on the barrier along the steel braided cables (Figure 3), fixed with steel clamps.

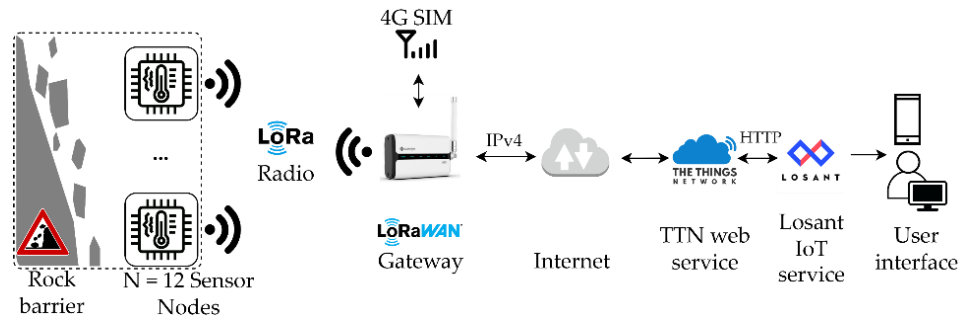


Figure 2. Proposed system application scheme.

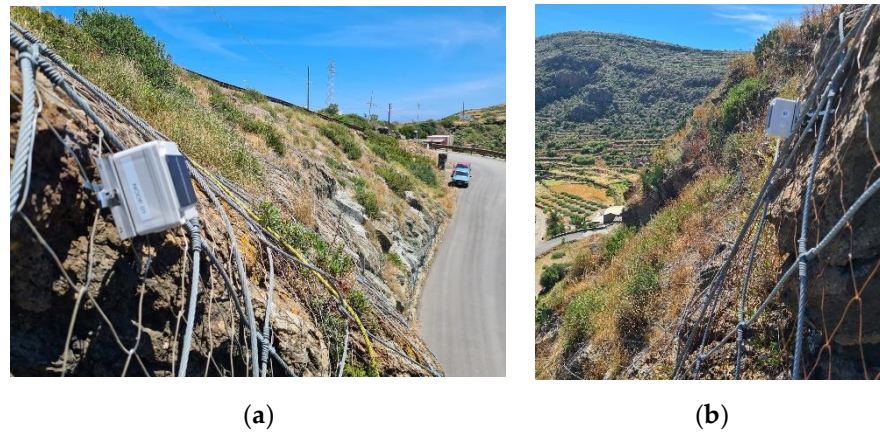


Figure 3. Nodes installation pictures: (a) node on roadside slope rock formation; and (b) node installation on a hillside above a beach area.

With the nodes placed at different heights and positions, the LoRa connectivity is provided with two gateways at different locations to enable all the 12 sensing devices to have radio communication. The gateways are placed in a position where the LTE connection is achievable, as the cellular connection in the island is not accessible everywhere, and where sunlight is available during a good portion of daytime (Figure 4).



Figure 4. Gateway installation.

3. Hardware Structure

In this section the hardware of the sensor nodes and gateways will be described. An analysis of power consumption is reported.

3.1. Sensor Node Structure and Power Analysis

The nodes are electronic circuits composed of a co-ordinator microcontroller, movement and environmental sensors, global positioning system (GPS) modem, an UART to USB interface, battery management unit connected to a 5 V solar panel, and a power supply and distribution chain. The microcontroller is a STM32L [52] from STMicroelectronics, 32-bit ARM Cortex M3-based, specified for low power applications. The low-power run mode of this microcontroller unit (MCU) with few microamperes specified makes it particularly suitable to battery powered applications, hence harvesting-based WSNs. The chip is equipped with multiple universal asynchronous receiver-transmitter (UART) channels, two different serial peripheral interface (SPI) ports, and two inter-integrated circuit (I²C) interfaces. In phase of debug and programming, it is possible to use a universal serial bus (USB) 2.0 compliant interface by means of a CP2102 UART to USB circuit from Silicon Labs [53]. This device works with COM communication port computer applications and is powered by the USB bus at 5 V, accessible at the micro-USB connector. The battery is a 3700 mAh lithium polymer (LiPo) battery. The voltage is readable using the analog to digital converter (ADC) of the microcontroller. The cell is charged using solar harvesting or directly from the USB port by means of a BQ21040 [54] single cell charging integrated circuit from Texas Instruments (TI). It is packaged in a SOT-23 case and supports a charge current up to 0.8 A at 4.2 V charging voltage. Thermal protection needs an external NTC resistor on the battery case to protect in case of excessive battery temperature. Most of the circuits in the sensor node are powered at 3.3 V by means of a RP104N331 [55] low drop-out (LDO) regulator by Nisshinbo. The GPS modem onboard is a Ublox MAX-7Q [56], powered at 3.3 V, switched using a TI TPS27082 [57] load switch. It communicates with the MCU using UART. The movement sensor is a MEMS based digital output three-axis accelerometer mode LIS3DH [58] from STMicroelectronics, supporting low power mode with a current consumption of around 2 μ A. The chip is interfaced with the microcontroller by I²C and supplied at 3.3 V.

The LoRa module is SX1276 [59] from Semtech, a transceiver for long-range technology that implements the spread spectrum communication patented by Semtech. It is interfaced with the microcontroller using SPI and supplied at 3.3 V. SX1276 can achieve a sensitivity of over -148 dBm using a low-cost crystal, moreover this integrated circuit is available on the market at a reduced cost. The unit is operating at transmission (TX) power of 13 dBm. To enable radio communication, an 868 MHz ISM band planar dipole antenna model PIOV008NRAA-100 [60], from Amphenol, is connected to the wireless module by a U.FL surface mount connector. The operating temperature of the nodes ranges from -40 °C to $+85$ °C. The barometric pressure is kept at the same value of external ambient, thanks to a compensation valve. In Figure 5, the sensor node block scheme is reported.

The node operates in sequential operation. At first, the device is in standby mode; this means that the onboard circuits are put in low power mode to enable reduced current absorption. At fixed time intervals selectable by the user, there is standby deactivation, and a data acquisition procedure begins. GPS position fetching is the initial procedure. If the GPS signal is not found until 30 s timeout reaching, other satellite connections are attempted, otherwise the node proceeds with sensor reading. Data from the movement sensor and environmental unit are retrieved, after which a data transmission phase begins, using LoRa interface. After data sending is concluded, the node will return to low power mode. If the LoRa network is not accessible in the sending phase, after a count of eight tries at gateway connection, the node will return to standby mode until next data sending scheduled interval. This procedure is valid for all the sensor nodes in the WSN.

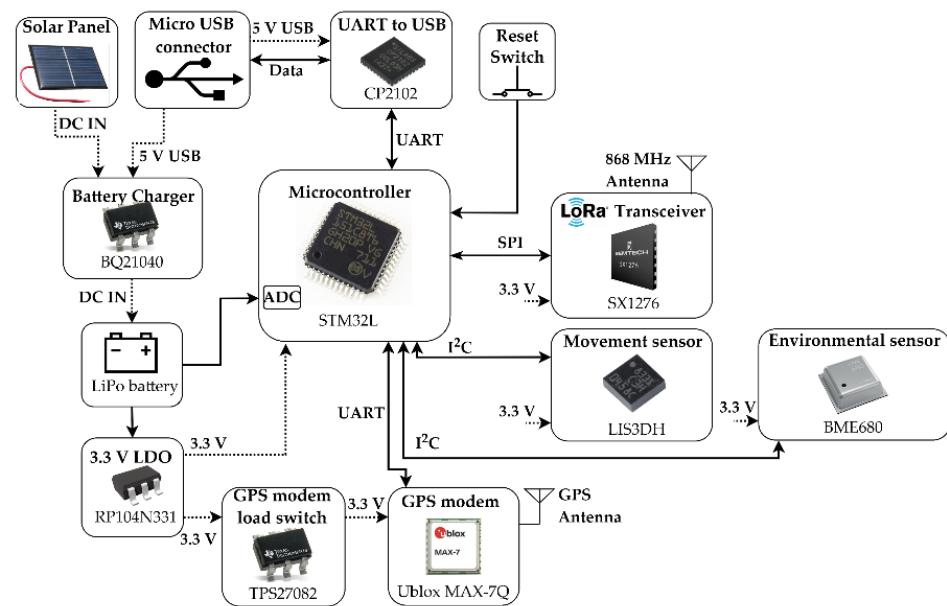


Figure 5. Sensor node block scheme.

In Figure 6 a flow diagram of the nodes’ operation is reported with the aforementioned operating stages pictured. The power on represents the moment when power supply is connected, followed by the first initialization which is executed only after every reset or power on.

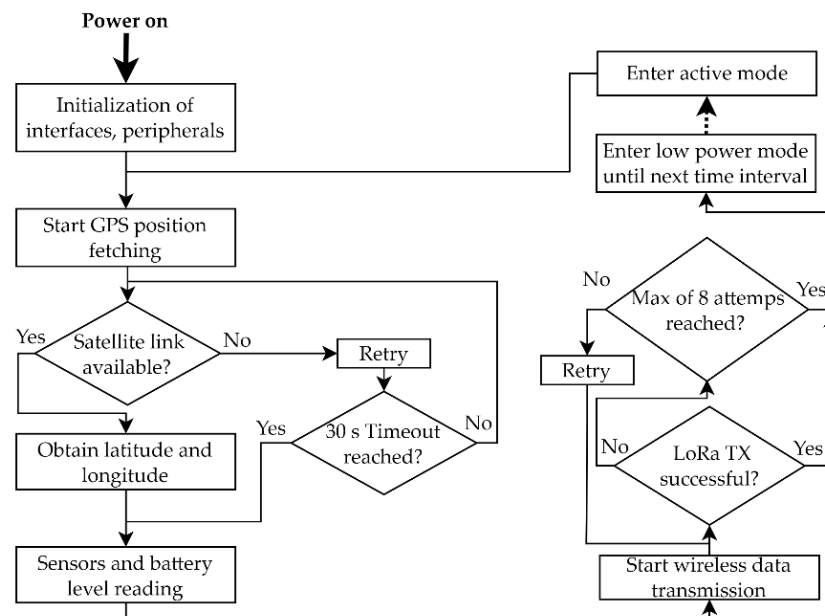


Figure 6. Sensor node operation flow diagram.

Power consumption of the sensor nodes is relevant to battery duration, it is therefore necessary to reduce current absorption during low power mode to ensure energetic sufficiency. Measurements were carried out to check the power draw of the node using an ultra-precise current monitor setup based on INA229 [61], from TI. The integrated circuit is interfaced using SPI, with a microcontroller model SAMD21 from Microchip [62], used to manage the readout and to communicate the data towards a personal computer using the COM port. The sensor node is put in series with a shunt resistor selected to read the absorbed current I_{node} , that represents the current drawn from the LiPo battery. A schematic of the setup is reported in Figure 7.

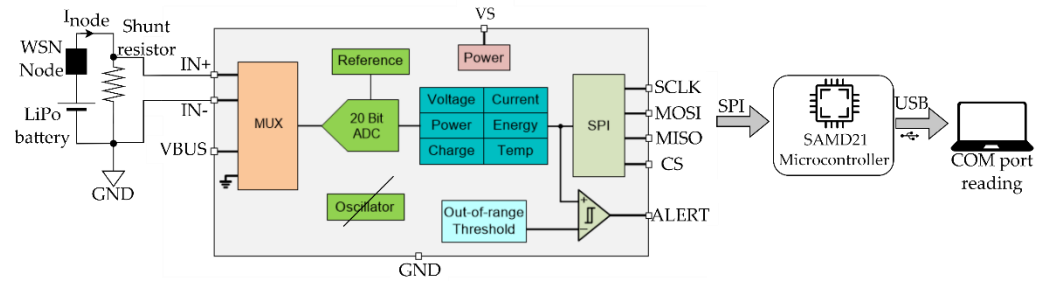


Figure 7. Measurements setup for the current absorption of one sensor node.

In Figure 8, a graph reporting the current absorption in mA (vertical axis) during data sending attempts is reported over a time interval of 50 s (horizontal axis) at 3.8 V battery voltage. The node will not reach a gateway, therefore several connection efforts are attempted. It operates at an average active current of 35.7 mA, following which is the standby mode activation, where the current absorption drops to an average value of $I_{LP} = 16 \mu\text{A}$. In Figure 8, it is also possible to observe the current peaks due to transmission attempts.

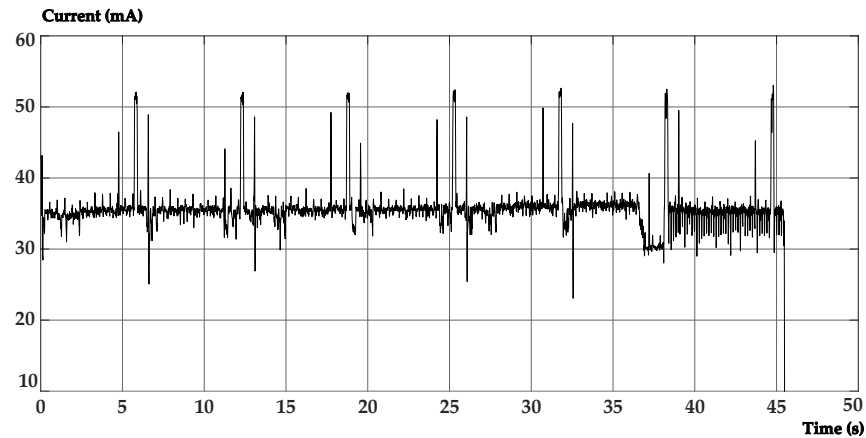


Figure 8. Current absorption graph during LoRa TX attempts of the sensor node.

The total duration of one acquisition cycle is 60 min long, during a successful attempt of wake-up, GPS data retrieving and LoRa transmission, in case of satellite reachability, for a time span of about $T_{ACT} = 15 \text{ s}$. This estimates a low power operation mode of 3585 s over one activity cycle. The average current absorption maintains at $I_{ACT} = 35.7 \text{ mA}$, being the LoRa transceiver and GPS unit absorption peaks, which are very narrow in time. The single 1 h cycle battery discharge due to the activity is given by:

$$C_{ACT} = (T_{ACT} \cdot I_{ACT})/3600 = 0.148 \text{ mAh} \tag{1}$$

The discharge in one cycle due to the low power mode is the following, where T_{LP} is the sleep time per cycle that is 45 s:

$$C_{LP} = (T_{LP} \cdot I_{LP})/3600 = 0.0002 \text{ mAh} \tag{2}$$

One day of operation, multiplying the total discharge of one cycle by 24, gives a discharge of about 3.56 mAh. In one year of operation, multiplying the daily discharge by 365 days, there is a discharge of about $C_Y = 1300 \text{ mAh}$. This results in a total battery duration, in case of an ideal steady battery state, of around 2.8 years in case of total darkness where solar harvesting is not working. For the node-obtained data that will be illustrated in the sequent section, the battery remains almost fully charged for all the working time, thanks to the solar panel implementation, which gives the sensor nodes a sufficient level of energy.

3.2. Gateway Assembly

The two LoRaWAN gateways provide access to the internet layer through The Things Network service, as described above. The gateways are model UG65 [63] from Milesight, powered at 12 V direct current (DC) using a valve-regulated lead-acid battery. It is based on a 64-bit 1.5 GHz ARM Cortex A53 processor, supported by 512 MB of DDR4 RAM and a flash memory of 8 GB. It supports external and internal antennas, with an output power at the output stage for LoRaWAN of 27 dBm and a sensitivity of -140 dBm. The working band is EU868 which stands for European band, with a center frequency of 868 MHz. The LTE-interfaced gateways are assembled in a waterproof IP65 enclosure with the supply system. The rated typical total power of the gateway is 2.9 W. The operating temperature range of the gateways is -40 °C to $+70$ °C.

The solar panel is a IP65 polycrystalline type, model NX30P from Energiasolare100 [64], with 344 mm length, 645 mm width and 25 mm height. The weight is 2.4 kg for the whole package in aluminum frame. The peak power is 30 W, and it reports an open circuit voltage of around 21 V. The battery charge regulator is an EP5 [65] model PWM-based device. It features overcurrent and reverse polarity protection, working at 13.8 V battery charge, retaining voltage. The storage is implemented using a PCA12-12 [66] battery from Prime, which powers the LoRaWAN gateway through a DC jack. In Figure 9, the gateway mounting scheme is reported.

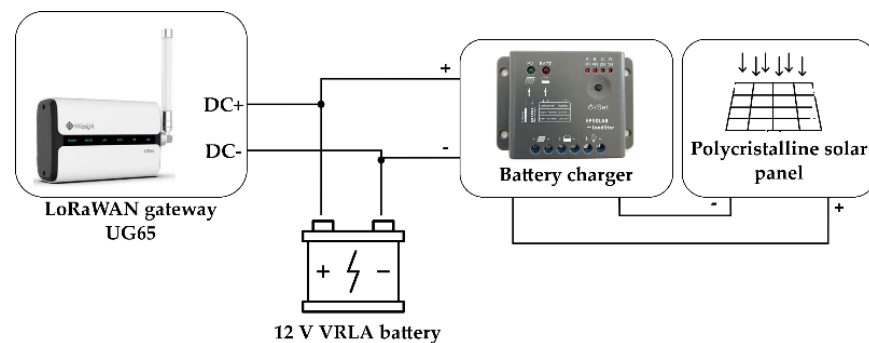


Figure 9. LoRaWAN gateway mounting schematic.

4. Measured Data

The system is in operation with a full uptime. However, it is possible to observe that not all the nodes are able to transmit the same quantity of data, as some are situated in locations where the LoRa signal does not always reach the gateway successfully. For this reason, some nodes will report an inferior number of points per data graph over the same time period.

The GPS unit allows tracking of the sensor nodes. This is useful in different cases: locating a node for maintenance, position acknowledgment in case of rockfall events, and to enable the fastest and more effective risk-reduction-technique and hazard plan. In case of vandalism, it is possible to locate the node, if it is active, by following the tracked GPS position. In Figures 10 and 11 some pictures showing the location of the sensor nodes in Pantelleria Island are given.

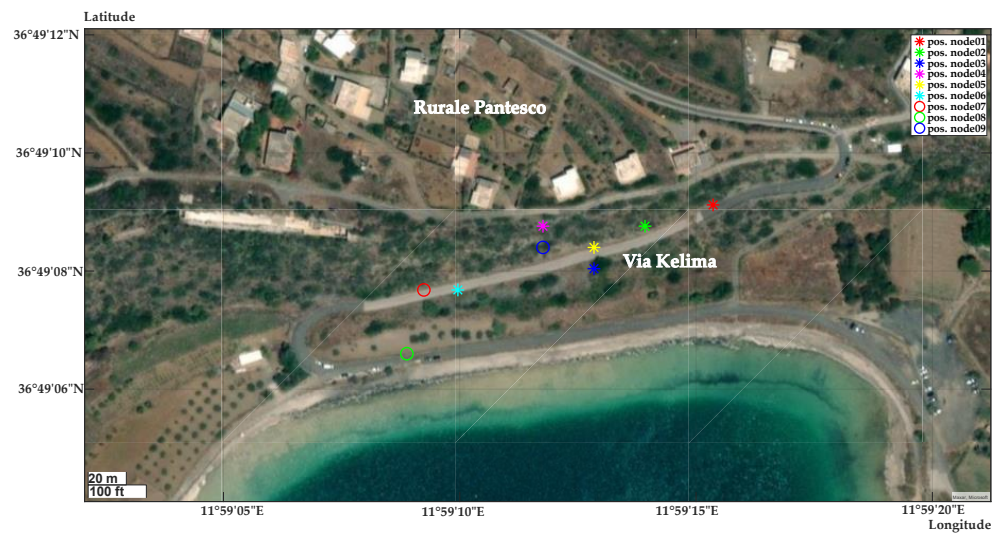


Figure 10. Sensor nodes 01–09 in Rurale Pantesco, via the Kelima area.



Figure 11. Sensor nodes 10, 11, 12 in the Hot Springs area.

Some data plots (Figures 12–24) are reported. They are related to the period 1–25 July 2022.

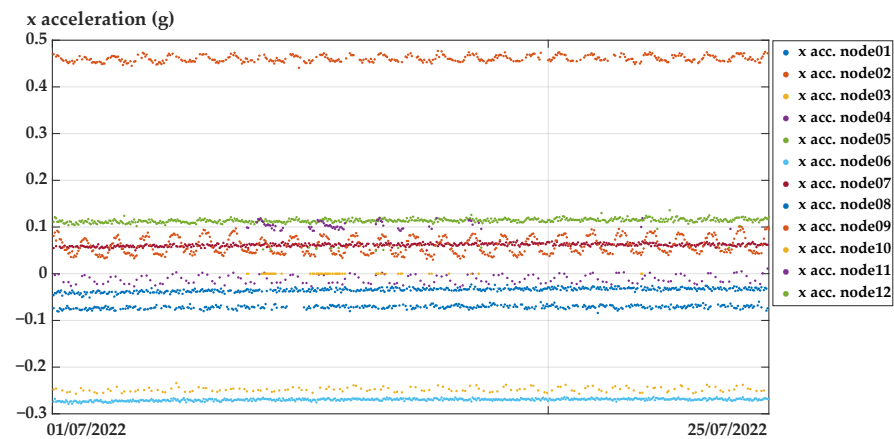


Figure 12. Measured x axis acceleration for all the nodes from 1 July 2022 to 25 July 2022.

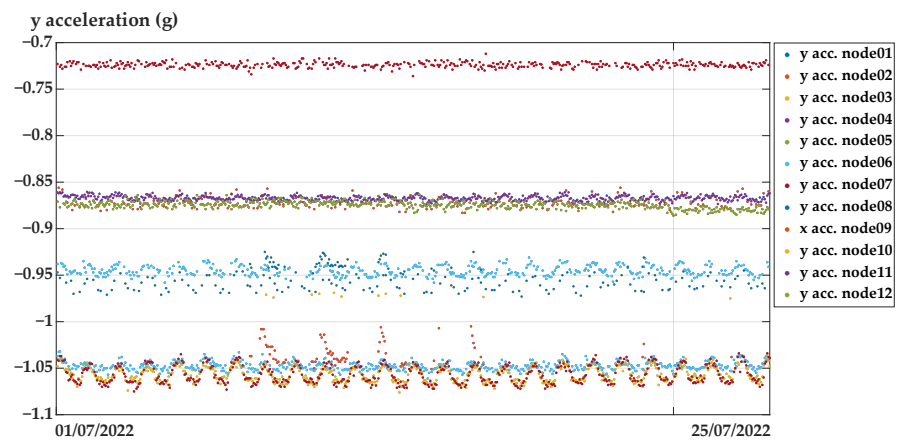


Figure 13. Measured y axis acceleration for all the nodes from 1 July 2022 to 25 July 2022.

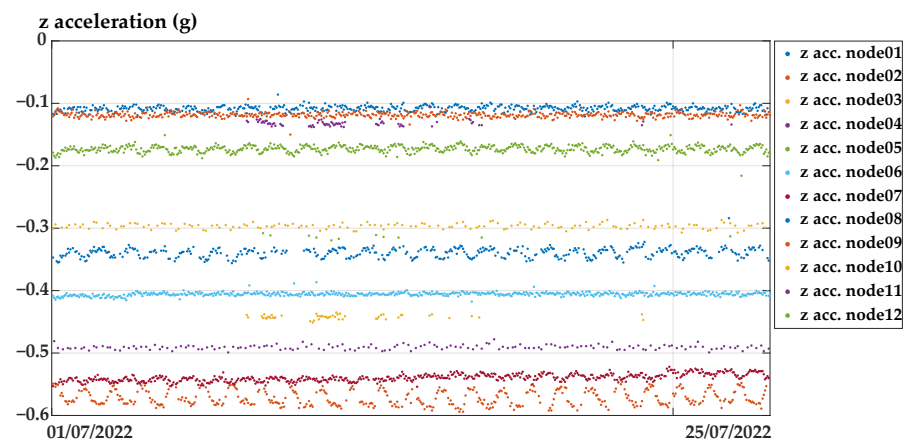


Figure 14. Measured z axis acceleration for all the nodes from 1 July 2022 to 25 July 2022.

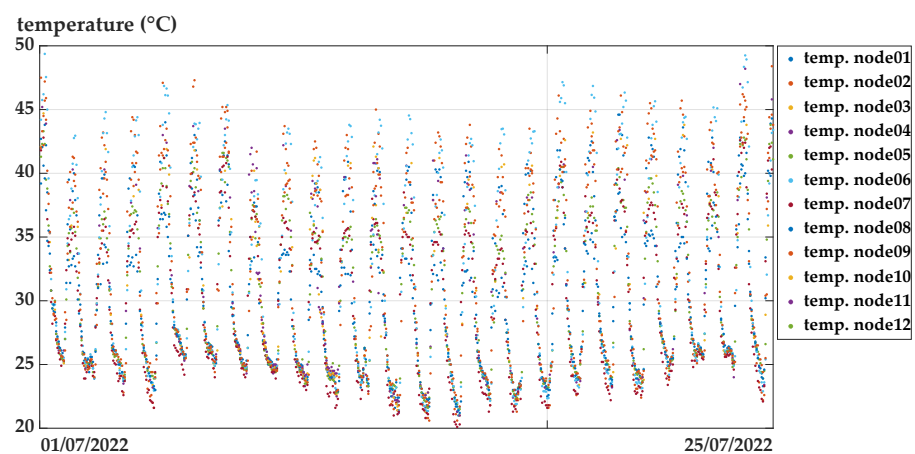


Figure 15. Measured temperature for all the nodes from 1 July 2022 to 25 July 2022.

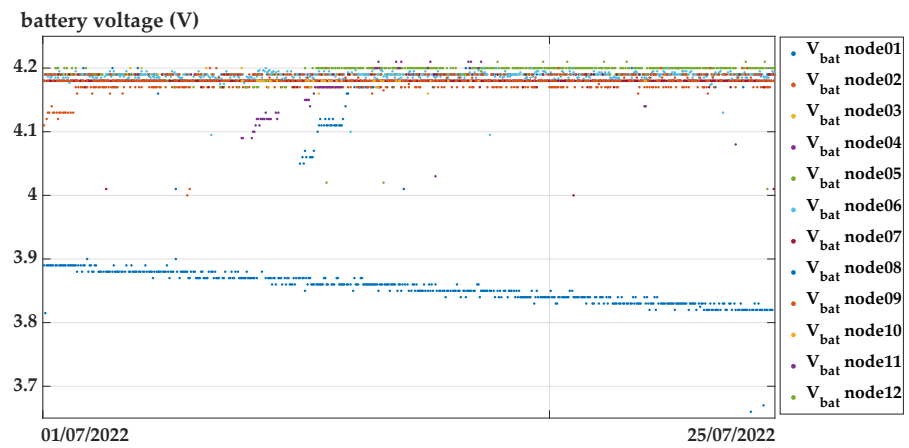


Figure 16. Measured battery voltage for all the nodes from 1 July 2022 to 25 July 2022.

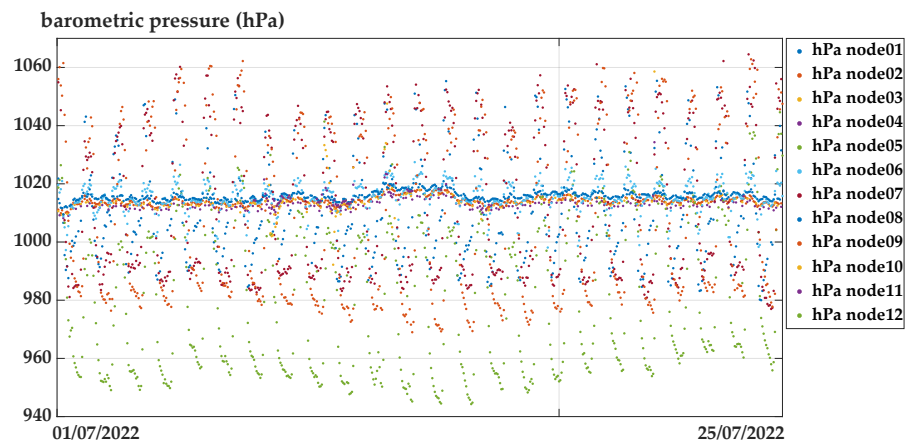


Figure 17. Measured barometric pressure for all the nodes from 1 July 2022 to 25 July 2022.

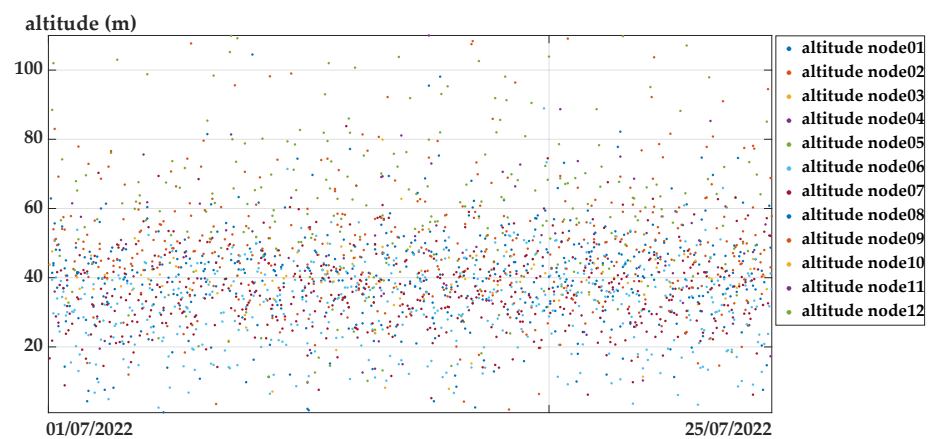


Figure 18. Measured altitude for all the nodes from 1 July 2022 to 25 July 2022.

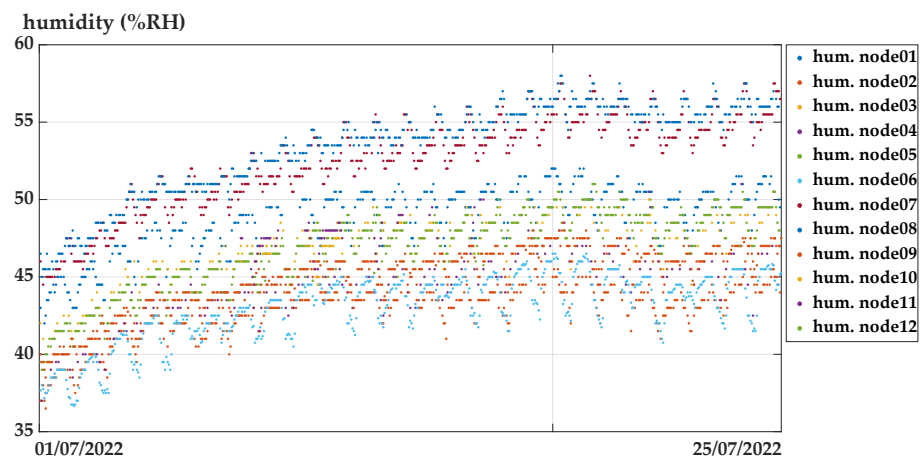


Figure 19. Measured relative humidity for all the nodes from 1 July 2022 to 25 July 2022.

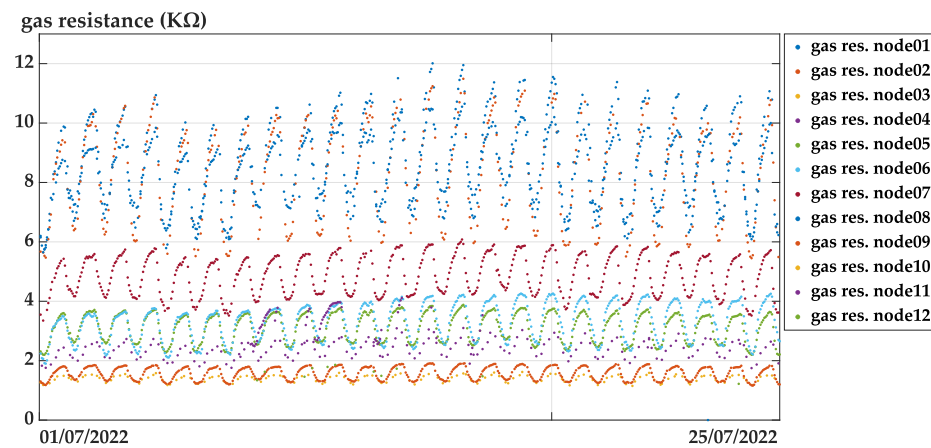


Figure 20. Measured gas resistance parameter for all the nodes from 1 July 2022 to 25 July 2022.

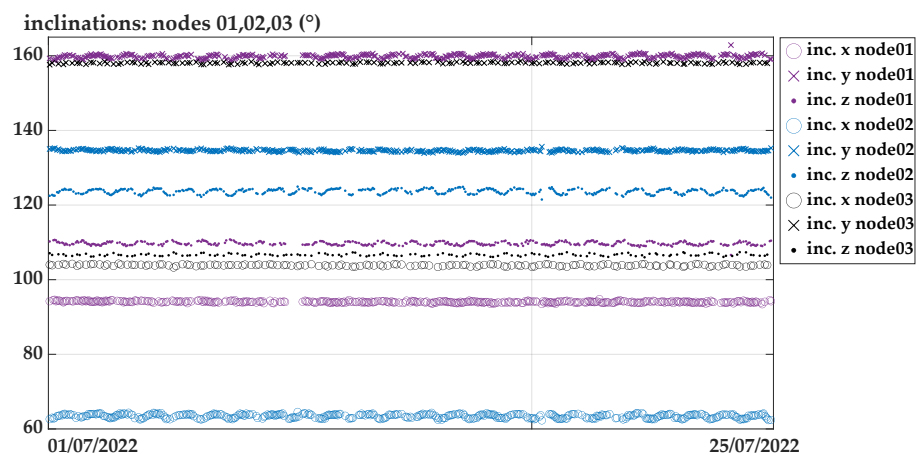


Figure 21. Inclination along x, y, and z axes for nodes 01–03 from 1 July 2022 to 25 July 2022.

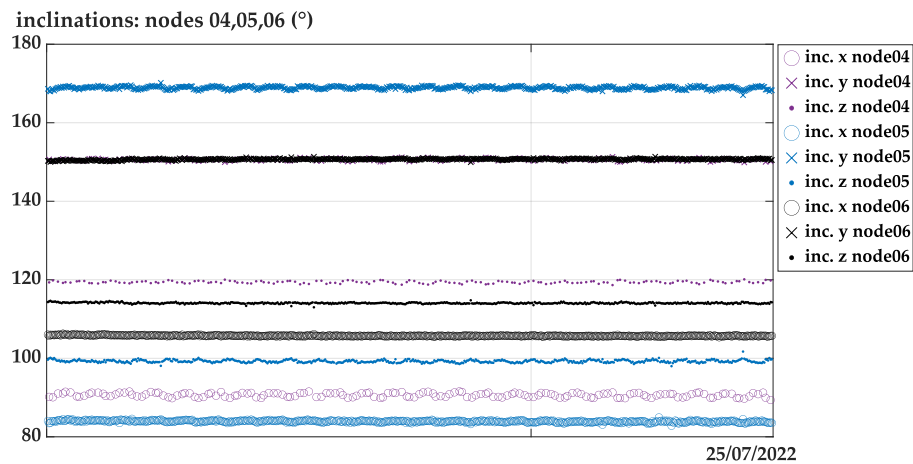


Figure 22. Inclination along x, y, and z axes for nodes 04–06 from 1 July 2022 to 25 July 2022.

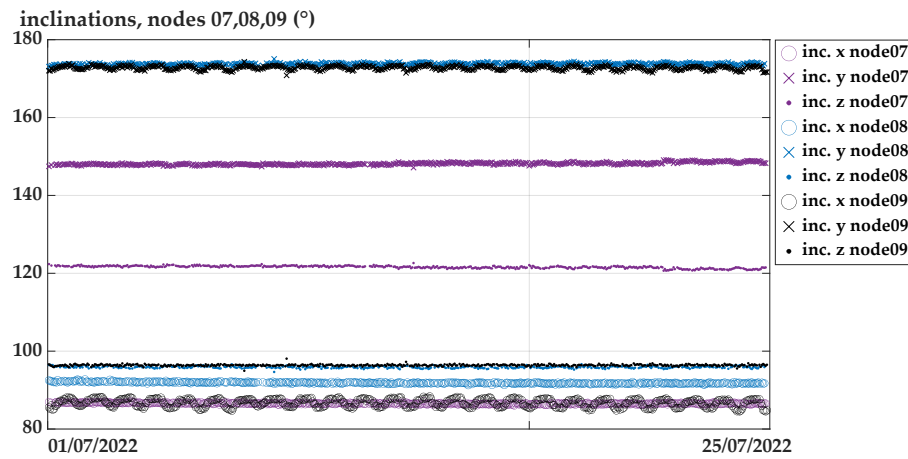


Figure 23. Inclination along x, y, and z axes for nodes 07–09 from 1 July 2022 to 25 July 2022.

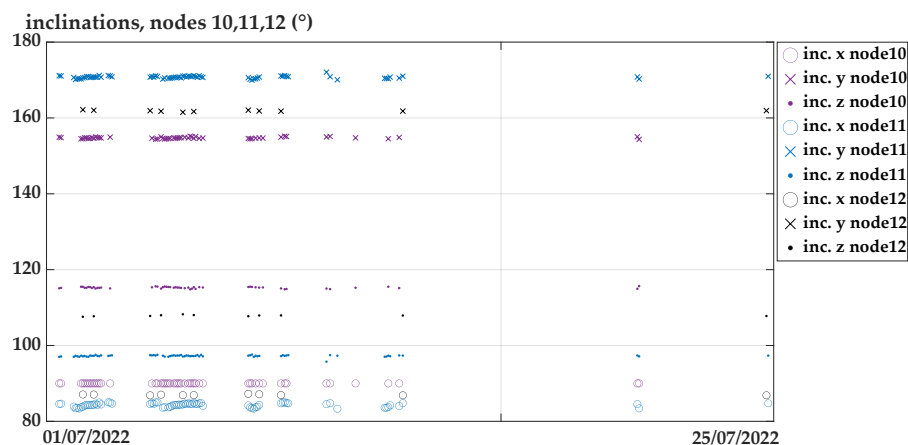


Figure 24. Inclination along x, y, and z axes for nodes 10–12 from 1 July 2022 to 25 July 2022.

Due to the effectiveness of solar harvesting, it is possible to observe (see Figure 16) the average value of battery voltage for 12 nodes of about 4.14 V, which is almost full level. Only one node (node 08) reports a descending battery voltage, meaning that the light is not enough to activate the charging mechanism. The maintenance operators can monitor the status of the battery and charge the node when needed. The acceleration values formula (Figures 12–14) have been used to obtain inclination values in degrees along the axes using the following. In this case, INC_x means x axis inclination, a_x , a_y , a_z accelerations along

x , y , and z axes expressed in $\frac{m}{s^2}$. Inclinations along the other two axes are calculated by substituting the acceleration value at the numerator of \cos^{-1} with the acceleration on the desired axes.

$$INC_x = \frac{180 \cdot (\cos^{-1}(\frac{a_x}{\sqrt{a_x^2 + a_y^2 + a_z^2}}))}{\pi} \quad (3)$$

The measured temperature is the internal temperature in the sensor nodes box (Figure 15). In Figures 17 and 18 the received barometric pressure and altitude data are reported. Relative humidity received from the 12 nodes is observable in Figure 19. The gas resistance value (Figure 20) is currently indicated as standalone information but can, as previously stated, be used to calculate AQI using Bosch's Software.

Inclination values along the three axes are plotted in the graphs in Figures 21–24. All the considered WSN nodes use the adaptive data rate (ADR) [67,68] feature of LoRaWAN, a mechanism for optimizing data rates, airtime, and energy consumption. The network server indicates to the end device to modify its transmission parameters in order to achieve minor airtime, hence power consumption, on the basis of the received signal intensity and signal to noise ratio (SNR). It is possible to observe (Figure 24) that the nodes 10, 11, 12 do not benefit from an ideal LoRa connection with the gateway, as some packets were missed during the considered time span. However, due to the portability of the gateway assembly, it is possible to find the optimal point for reception. The system is currently operating under tests to achieve better performances.

The described system allows for flexibility of the WSN thanks to its fully portable nature with respect to the aforementioned state-of-the-art implementations, such as [18] where a trailer with a computer is necessary for cellular network access. The key factor is the use of free access MAC layer through The Things Network Stack service, which enables a faster and cheaper implementation of the system. Moreover, being the aforementioned platform for LoRaWAN users rapidly spreading across all the planet, there is a strong emphasis on development which leads to up-to-date features, both in terms of modularity and security. Security is, in fact, granted in LoRaWAN by standardized cryptographic AES algorithms [69]. In custom implementations, such as the one previously described in [23], the structures for data exchange between platforms and post processing can be implemented in various manners. In a low-cost WSN this should be addressed in the most economically efficient manner as possible. For this reason, the present study implements web services which are freely accessible, demonstrating how it is feasible to implement fully working systems with low expenses. Moreover, the modularity of the system benefits from using standalone building blocks: the sensor nodes can be equipped with different and various hardware, but the LoRa blocks from the transmission stage forward can remain the same.

5. Conclusions

In this paper, a standalone rockfall and landslide monitoring system, with enhanced environmental monitoring capabilities, was presented, covering the hardware, firmware, and software design of a remote monitoring system, implementing it on low cost hardware and giving a complete view of a real scenario installation. For each element, the following parameters have been monitored: axial accelerations, temperature, barometric pressure, altitude, relative humidity, gas resistance for air AQI, and battery level. The system is composed of sensor nodes which communicate with gateways in star topology through the LoRa wireless modulation technique, forming a wireless sensor network structure. The WSN was installed in a real scenario, in Pantelleria Island, on rockfall barriers in two risk-subjected locations. The monitoring system is operating in support of safety for local viability and hazard reduction. The hardware structure of nodes was presented, along with the gateway system which allows portable LoRaWAN access using cellular connectivity. Power consumption measurements of the nodes are reported, with considerations on the energetic performances, reporting an energy sufficiency estimated at 2.8 years in absence of solar harvesting interventions. Experimental data extracted from the web user interface are provided for the period of July 2022, showing the measured parameters for different sensor

nodes. The inclinations along three special axes, calculated using accelerometric data, do not show significant rockfall events in the reported period. As the sensing elements are placed in two groups at distances that do not allow the environmental conditions to vary in significantly observable manner, the recorded environmental data over the sample period is similar for all the nodes. It is possible to observe different behavior in radio communication due to the unfavorable position of nodes 10–12, with respect to the LoRaWAN gateway. Future developments of this work will be in the optimization of packet transmission in terms of packet loss (as it is possible to observe that nodes that do not successfully reach a gateway introduce information losses), possibly implementing different resource allocation algorithms, such as retransmission-assisted resource management [70]. Other future works will be the introduction of different sensors in the nodes to develop a yet more multifunction-oriented low-cost device.

Author Contributions: Conceptualization, M.R. and V.S.; methodology, M.R. and V.S.; software, M.R., G.B. and V.S.; validation, M.R. and V.S.; formal analysis, M.R. and V.S.; investigation, M.R.; resources, M.R. and V.S.; data curation, M.R. and V.S.; writing—original draft preparation, M.R.; writing—review and editing, M.R., G.F. and V.S.; visualization, M.R. and G.F.; supervision, A.L., G.B., G.F. and V.S.; project administration, V.S.; funding acquisition, V.S. All authors have read and agreed to the published version of the manuscript.

Funding: This research was funded by Frutti Carlo M+M, brand We.Monitoring.HA.

Data Availability Statement: The data presented in this study are available on request from the corresponding author. The data are not publicly available due to privacy policies.

Acknowledgments: The authors acknowledge Frutti Carlo M+M, WeMonitoring brand, Gheller S.r.l., Fox S.r.l., Sofia Costruzioni S.r.l., Government commissioner against hydrogeological instability in the Sicilian Region ex legibus n° 116/2014 and n° 164/2014, and the municipality of Pantelleria.

Conflicts of Interest: The authors declare no conflict of interest.

References

1. Luuk, K.A. Dorren: A review of rockfall mechanics and modelling approaches. *Prog. Phys. Geogr.* **2003**, *27*, 69–87. [[CrossRef](#)]
2. Calista, M.; Menna, V.; Mancinelli, V.; Sciarra, N.; Miccadei, E. Rockfall and Debris Flow Hazard Assessment in the SW Escarpment of Montagna del Morrone Ridge (Abruzzo, Central Italy). *Water* **2020**, *12*, 1206. [[CrossRef](#)]
3. Rossi, M.; Guzzetti, F.; Salvati, P.; Donnini, M.; Napolitano, E.; Bianchi, C. A predictive model of societal landslide risk in Italy. *Earth-Sci. Rev.* **2019**, *196*, 102849. [[CrossRef](#)]
4. SMineo, S.; Pappalardo, G.; D'Urso, A.; Calcaterra, D. Event tree analysis for rockfall risk assessment along a strategic mountainous transportation route. *Environ. Earth Sci.* **2017**, *76*, 620. [[CrossRef](#)]
5. Chau, K.T.; Wong, R.H.C.; Liu, J.; Lee, C.F. Rockfall Hazard Analysis for Hong Kong Based on Rockfall Inventory. *Rock Mech. Rock Eng.* **2003**, *36*, 383–408. [[CrossRef](#)]
6. Mattia, M.; Bonaccorso, A.; Guglielmino, F. Ground deformations in the Island of Pantelleria (Italy): Insights into the dynamic of the current interruptive period. *J. Geophys. Res.* **2007**, *112*, B11406. [[CrossRef](#)]
7. Ishikawa, K.-I.; Mita, A. Time synchronization of a wired sensor network for structural health monitoring. *Smart Mater. Struct.* **2008**, *17*, 15016. [[CrossRef](#)]
8. Paolucci, R.; Muttillio, M.; Di Luzio, M.; Alaggio, R.; Ferri, G. Electronic Sensory System for Structural Health Monitoring Applications. In Proceedings of the 2020 5th International Conference on Smart and Sustainable Technologies (SpliTech), Split, Croatia, 23–26 September 2020. [[CrossRef](#)]
9. Mainetti, L.; Patrono, L.; Vilei, A. Evolution of Wireless Sensor Networks towards the Internet of Things: A Survey. In Proceedings of the SoftCOM 2011, 19th International Conference on Software, Telecommunications and Computer Networks, Split, Croatia, 15–17 September 2011.
10. Puccinelli, D.; Haenggi, M. Wireless sensor networks: Applications and challenges of ubiquitous sensing. *IEEE Circuits Syst. Mag.* **2005**, *5*, 19–29. [[CrossRef](#)]
11. Oliveira, L.M.; Rodrigues, J.J. Wireless Sensor Networks: A Survey on Environmental Monitoring. *J. Commun.* **2011**, *6*, 143–151. [[CrossRef](#)]
12. Darwish, A.; Hassanien, A.E. Wearable and Implantable Wireless Sensor Network Solutions for Healthcare Monitoring. *Sensors* **2011**, *11*, 5561–5595. [[CrossRef](#)] [[PubMed](#)]
13. Ragnoli, M.; Barile, G.; Leoni, A.; Ferri, G.; Stornelli, V. An Autonomous Low-Power LoRa-Based Flood-Monitoring System. *J. Low Power Electron. Appl.* **2020**, *10*, 15. [[CrossRef](#)]

14. Aponte-Luis, J.; Gómez-Galán, J.A.; Gómez-Bravo, F.; Sánchez-Raya, M.; Alcina-Espigado, J.; Teixido-Rovira, P.M. An Efficient Wireless Sensor Network for Industrial Monitoring and Control. *Sensors* **2018**, *18*, 182. [CrossRef]
15. Mei, G.; Xu, N.; Qin, J.; Wang, B.; Qi, P. A Survey of Internet of Things (IoT) for Geohazard Prevention: Applications, Technologies, and Challenges. *IEEE Internet Things J.* **2020**, *7*, 4371–4386. [CrossRef]
16. Barile, G.; Ferri, G.; Leoni, A.; Muttillio, M.; Pantoli, L.; Stornelli, V.; Vettori, D. Automatic Wireless Monitoring System for Real-Time Rock Fall Events. *Proceedings* **2017**, *1*, 569. [CrossRef]
17. Caviezel, A.; Schaffner, M.; Cavigelli, L.; Niklaus, P.; Buhler, Y.; Bartelt, P.; Magno, M.; Benini, L. Design and Evaluation of a Low-Power Sensor Device for Induced Rockfall Experiments. *IEEE Trans. Instrum. Meas.* **2018**, *67*, 767–779. [CrossRef]
18. Giri, P.; Ng, K.; Phillips, W. Wireless Sensor Network System for Landslide Monitoring and Warning. *IEEE Trans. Instrum. Meas.* **2019**, *68*, 1210–1220. [CrossRef]
19. Vassiss, D.; Kormentzas, G.; Rouskas, A.; Maglogiannis, I. The IEEE 802.11g standard for high data rate WLANs. *IEEE Netw.* **2005**, *19*, 21–26. [CrossRef]
20. Arosio, D.; Longoni, L.; Papini, M.; Scaioni, M.; Zanzi, L.; Alba, M. Natural Hazards and Earth System Sciences Towards rockfall forecasting through observing deformations and listening to microseismic emissions. *Nat. Hazards Earth Syst. Sci.* **2009**, *9*, 1119–1131. Available online: www.nat-hazards-earth-syst-sci.net/9/1119/2009/ (accessed on 24 August 2022).
21. Pakzad, S.N.; Fenves, G.L.; Kim, S.; Culler, D.E. Design and Implementation of Scalable Wireless Sensor Network for Structural Monitoring. *J. Infrastruct. Syst.* **2008**, *14*, 89–101. [CrossRef]
22. Crossbow Technology. *MicaZ Datasheet*; Document Part Number: 6020-0060-04 Rev A; Crossbow Technology: San Jose, CA, USA, 2011.
23. Tseng, K.-H.; Chung, M.-Y.; Chen, L.-H.; Huang, Y.-W. Implementation of Composite LPWAN on the Slope Disaster Prevention Monitoring System. *IEEE Sens. J.* **2022**, *22*, 2658–2671. [CrossRef]
24. Vangelista, L. Frequency Shift Chirp Modulation: The LoRa Modulation. *IEEE Signal Process. Lett.* **2017**, *24*, 1818–1821. [CrossRef]
25. Semtech. AN1200.22 LoRa™ Modulation Basics. Available online: <https://semtech.my.salesforce.com/sfc/p/#E0000000JelG/a/2R0000001OJu/xvKUC5w9yjG1q5Pb2IikpolW54YYqGb.frOZ7HQBcRc> (accessed on 24 August 2022).
26. Mangalvedhe, N.; Ratasuk, R.; Ghosh, A. NB-IoT deployment study for low power wide area cellular IoT. In Proceedings of the 2016 IEEE 27th Annual International Symposium on Personal, Indoor, and Mobile Radio Communications (PIMRC), Valencia, Spain, 4–8 September 2016; pp. 1–6. [CrossRef]
27. GSMA. *LTE-M Deployment Guide to Basic Feature Set Requirements*; GSMA: London, UK, 2019.
28. Hsieh, P.C.; Jia, Y.; Parra, D.; Aithal, P. An Experimental Study on Coverage Enhancement of LTE Cat-M1 for Machine-Type Communication. In Proceedings of the 2018 IEEE International Conference on Communications (ICC), Kansas City, MO, USA, 20–24 May 2018; pp. 1–5. [CrossRef]
29. Raspberry Pi 3 Product Description. Available online: www.rs-components.com/raspberrypi (accessed on 24 August 2022).
30. *MySQL 8.0 Reference Manual Including MySQL NDB Cluster 8.0*; Rev 73994; MySQL: Austin, TX, USA, 2022; Available online: <https://downloads.mysql.com/docs/refman-8.0-en.pdf> (accessed on 24 August 2022).
31. TECO Group, Tecom Co., LTD. Smart Vibration Gauge Solution. Available online: https://teco.com.sg/wp-content/uploads/2019/09/Vibration-Gauge_Eng_0904_v03.pdf (accessed on 24 August 2022).
32. B&B Electronics Manufacturing Company. RS-422 and RS-485 Application Note. Available online: <https://www.cpii.com/docs/library/4/485appnote.pdf> (accessed on 24 August 2022).
33. Romdhane, R.F.; Lami, Y.; Genon-Catalot, D.; Fourty, N.; Lagrèze, A.; Jongmans, D.; Baillet, L. Wireless sensors network for landslides prevention. In Proceedings of the 2017 IEEE International Conference on Computational Intelligence and Virtual Environments for Measurement Systems and Applications (CIVEMSA), Annecy, France, 26–28 June 2017; pp. 222–227. [CrossRef]
34. Wang, C.; Guo, W.; Yang, K.; Wang, X.; Meng, Q. Real-Time Monitoring System of Landslide Based on LoRa Architecture. *Front. Earth Sci.* **2022**, *10*, 899509. [CrossRef]
35. Sidorov, M.; Nhut, P.V.; Matsumoto, Y.; Ohmura, R. LoRa-Based Precision Wireless Structural Health Monitoring System for Bolted Joints in a Smart City Environment. *IEEE Access* **2019**, *7*, 179235–179251. [CrossRef]
36. Haxhibeqiri, J.; De Poorter, E.; Moerman, I.; Hoebeke, J. A Survey of LoRaWAN for IoT: From Technology to Application. *Sensors* **2018**, *18*, 3995. [CrossRef] [PubMed]
37. Semtech Corporation. LoRa and LoRaWAN: A Technical Overview, Technical Paper. 2020. Available online: https://lora-developers.semtech.com/uploads/documents/files/LoRa_and_LoRaWAN-A_Tech_Overview-Downloadable.pdf (accessed on 24 August 2022).
38. Ruan, T.; Chew, Z.J.; Zhu, M. Energy-Aware Approaches for Energy Harvesting Powered Wireless Sensor Nodes. *IEEE Sens. J.* **2017**, *17*, 2165–2173. [CrossRef]
39. Di Marco, P.; Stornelli, V.; Ferri, G.; Pantoli, L.; Leoni, A. Dual band harvester architecture for autonomous remote sensors. *Sens. Actuators A Phys.* **2016**, *247*, 598–603. [CrossRef]
40. Luo, P.; Peng, D.; Wang, Y.; Zheng, X. Review of Solar Energy Harvesting for IoT Applications. In Proceedings of the 2018 IEEE Asia Pacific Conference on Circuits and Systems (APCCAS), Chengdu, China, 26–30 October 2018; pp. 512–515. [CrossRef]
41. di Bernardo, G.; Narayana, A.; Hazarika, R. Choice of effective LPWAN protocol for IoT System: Sigfox and LoRa. *Int. J. Eng. Res. Appl.* **2020**, *10*, 53–57. [CrossRef]

42. Ragnoli, M.; Stornelli, V.; Del Tosto, D.; Barile, G.; Leoni, A.; Ferri, G. Flood monitoring: A LoRa based case-study in the city of L'Aquila. In Proceedings of the 2022 17th Conference on Ph.D Research in Microelectronics and Electronics (PRIME), Villasimius, Italy, 12–15 June 2022; pp. 57–60. [CrossRef]
43. Chaudhari, B.S.; Zennaro, M.; Borkar, S. LPWAN Technologies: Emerging Application Characteristics, Requirements, and Design Considerations. *Future Internet* **2020**, *12*, 46. [CrossRef]
44. Chaudhari, B.S.; Zennaro, M. *LPWAN Technologies for IoT and M2M Applications*; Academic Press: Cambridge, MA, USA, 2020.
45. LoRa Alliance. Available online: <https://lora-alliance.org/> (accessed on 24 August 2022).
46. Finnegan, J.; Brown, S. An Analysis of the Energy Consumption of LPWA-based IoT Devices. In Proceedings of the 2018 International Symposium on Networks, Computers and Communications (ISNCC), Rome, Italy, 19–21 June 2018; pp. 1–6. [CrossRef]
47. Sigfox. Sigfox Technical Overview. 2018. Available online: <https://www.avnet.com/wps/wcm/connect/onesite/03aebfe2-98f7-4c28-be5f-90638c898009/sigfox-technical-overview.pdf?MOD=AJPERES&CVID=magVa.N&CVID=magVa.N&CVID=magVa.N> (accessed on 24 August 2022).
48. Lauridsen, M.; Nguyen, H.; Vejlggaard, B.; Kovács, I.Z.; Mogensen, P.; Sorensen, M. Coverage Comparison of GPRS, NB-IoT, LoRa, and SigFox in a 7800 km² Area. In Proceedings of the 2017 IEEE 85th Vehicular Technology Conference (VTC Spring), Sydney, Australia, 4–7 June 2017; pp. 1–5. [CrossRef]
49. IBM. Internet Protocol Version 4 (IPv4). Available online: <https://www.ibm.com/docs/en/zos/2.3.0?topic=ipv6-internet-protocol-version-4-ipv4> (accessed on 24 August 2022).
50. The Things Network. Available online: <https://www.thethingsnetwork.org/> (accessed on 24 August 2022).
51. Losant IoT. Available online: <https://www.losant.com/> (accessed on 24 August 2022).
52. STMicroelectronics. *STM32L151x6/8/B STM32L152x6/8/B Ultra-Low-Power 32-Bit MCU Datasheet*; STMicroelectronics: Geneva, Switzerland, 2016.
53. SiliconLabs. *CP2102/9 Single-Chip Usb-to-Uart Bridge Datasheet*; Rev 1.8; SiliconLabs: Austin, TX, USA, 2017.
54. Texas Instruments. *bq21040 Datasheet*; Texas Instruments: Dallas, TX, USA, 2016.
55. Nisshinbo. *RP104x Series 150mA Ultra Low Supply Current LDO Regulator Datasheet*; NO. EA-150-161026; Nisshinbo: Tokyo, Japan, 2014.
56. U-Blox. *MAX-7 U-Blox 7 GNSS Modules Datasheet*; U-Blox: Thalwil, Switzerland, 2021.
57. Texas Instruments. *TPS27082L Datasheet*; Texas Instruments: Dallas, TX, USA, 2015.
58. STMicroelectronics. *LIS3DH MEMS Digital Output Motion Sensor: Ultra-Low-Power High-Performance 3-Axis 'Nano' Accelerometer Datasheet*; STMicroelectronics: Geneva, Switzerland, 2016.
59. Semtech. *SX1276/77/78/79—137 MHz to 1020 MHz Low Power Long Range Transceiver Datasheet*; Rev; Semtech: Camarillo, CA, USA, 2020.
60. Amphenol. *868MHz ISM Band PCB Antenna PIOV008NRA Datasheet*; Amphenol: Chicago, IL, USA, 2022; Available online: https://www.mouser.it/datasheet/2/18/1/Amphenol_04262021_PIOV008NRAA-2306547.pdf (accessed on 24 August 2022).
61. Texas Instruments. *INA229-Q1 Datasheet*; Texas Instruments: Dallas, TX, USA, 2021.
62. Microchip. *SAM D21/DA1 Family Low-Power, 32-Bit Cortex-M0+ MCU with Advanced Analog and PWM Features Datasheet*; Microchip Technology: Chandler, AZ, USA, 2020.
63. Milesight. UG65 LoRaWAN Gateway Datasheet. Available online: <https://resource.milesight-iot.com/milesight/document/ug65-datasheet-en.pdf> (accessed on 24 August 2022).
64. Energiasolare100. NX30P Solar Panel Datasheet. Available online: <https://www.dropbox.com/sh/mcz3qwx6hi3m9nl/AADHvhD5b3sFhH3AgLvU0r0Ba/01%20-%20Pannelli%20solari/Policristallino/NX30P.pdf?dl=0> (accessed on 24 August 2022).
65. Energiasolare100. Manuale d'uso Regolatore di Carica EP5 con Crepuscolare. Available online: <https://www.dropbox.com/sh/mcz3qwx6hi3m9nl/AACrlorx6dmQF9nT8SkP4wvpa/04%20-%20Regolatori%20di%20carica/EP%20Solar/EP5.pdf?dl=0> (accessed on 24 August 2022).
66. Energiasolare100. PCA12-12 Battery AGM Deep Cycle Datasheet. Available online: <https://www.dropbox.com/sh/mcz3qwx6hi3m9nl/AADG5pmgB5Vle1b5d6IoMTdJa/03%20-%20Batterie/AGM/PCA12-12.pdf?dl=0> (accessed on 24 August 2022).
67. Li, S.; Raza, U.; Khan, A. How Agile is the Adaptive Data Rate Mechanism of LoRaWAN? In Proceedings of the 2018 IEEE Global Communications Conference (GLOBECOM), Abu Dhabi, United Arab Emirates, 9–13 December 2018.
68. Semtech. *Understanding the LoRa® Adaptive Data Rate Technical Paper*; Semtech: Camarillo, CA, USA, 2019.
69. Eldefrawy, M.; Butun, I.; Pereira, N.; Gidlund, M. Formal security analysis of LoRaWAN. *Comput. Netw.* **2019**, *148*, 328–339. [CrossRef]
70. Farhad, A.; Kim, D.-H.; Pyun, J.-Y. R-ARM: Retransmission-Assisted Resource Management in LoRaWAN for the Internet of Things. *IEEE Internet Things J.* **2022**, *9*, 7347–7361. [CrossRef]